Contents lists available at SciVerse ScienceDirect

# Microelectronic Engineering

journal homepage: www.elsevier.com/locate/mee

# Inkjet-printed polymer–fullerene blends for organic electronic applications

M. Neophytou [a,b], W. Cambarau [b], F. Hermerschmidt [a], C. Waldauf [b], C. Christodoulou [a], R. Pacios [b], S.A. Choulis [a,*]

[a] *Molecular Electronics and Photonics Research Unit, Department of Mechanical Engineering and Materials Science and Engineering, Cyprus University of Technology, 3603 Limassol, Cyprus*
[b] *Department of Microsystems, IK4-IKERLAN S. Coop., Polo de Innovación Garaia, Goiru 9, E-20500 Arrasate-Mondragon, Spain*

## ARTICLE INFO

## ABSTRACT

Organic field effect transistors, photodiodes and solar cells based on polymer–fullerene blend active layers are printed electronic applications under intense studies. We show that the viscosity of the inkjet formulation, substrate temperature, drop spacing and the height of the droplet in relation to the surface are critical parameters to achieving high quality inkjet-printed polymer–fullerene based active layers. The effect of the above processing parameters on the performance of polymer–fullerene based organic solar cells is presented.

© 2012 Elsevier B.V. All rights reserved.

## 1. Introduction

Organic semiconductors are of increasing interest as new materials for electronic applications due to their easy processing – offering the potential for low fabrication cost [1–4]. Organic field effect transistors, photodiodes and solar cells based on polymer–fullerene blends are amongst the best performing organic electronic devices. The application of printing technology as a fabrication tool for organic electronic devices indicates the potential of these novel materials for low cost future electronic and optoelectronic applications. Understanding and gaining control over the printing process is an essential step for the commercialization of low cost organic photovoltaics, field effect transistors and photodiodes. In particular organic photovoltaics (OPVs) are lightweight and flexible and offer many new applications for solar cells, ranging from self-powered electronic newspapers to self-sufficient buildings [5–7].

At present, so-called bulk hetero-junction structures based on blends of a conjugated polymer as donor and a soluble fullerene derivative as acceptor represent the material system with the highest power conversion efficiency reported until now. Bulk hetero-junction (BHJ) type devices based on blends of regioregular poly(3-hexylthiophene) (RR-P3HT) and [6,6]-phenyl C61 butyric acid methyl ester (PCBM) provide power conversion efficiencies

(PCE) in the range of 3–4.5% [8,9]. Recently, power conversion efficiencies in the range of 6–8% have been achieved by using newly developed conjugated polymer donors blended with fullerene derivatives [10–12].

Most attempts to process highly efficient OPVs have focused on traditional coating techniques. For over a decade since the first BHJ devices were reported, all significant improvements in their power conversion efficiency occurred by control over their morphological properties. Main findings to control the morphology of RR-P3HT:PCBM solar cells fabricated by spin coating, doctor blading or spray coating techniques include optimization of the chemical properties of the polymer donor, processing/drying conditions and the effect of additives [13–27]. The first trials for inkjet printed OPVs using pristine solvents showed limited power conversion efficiency due to morphological limitations [28]. We note that previous work on organic field effect transistors (OFETs) and organic light emitting diodes (OLEDs) based on pristine organic semiconductor materials using inkjet printers were not subject to morphological limitations, since such devices usually did not require a two component material system [29,30]. This is now relevant for OPVs, photodiodes and ambipolar field effect transistors where the ink-formulation consists of multiple material components.

The first highly efficient organic solar cell by inkjet printing was reported by adjusting the chemical properties of a poly(3-hexylthiophene) polymer donor [31] and by using a novel inkjet solvent mixture [32]. Based on this work, control over the nano-morphology of poly(3-hexylthiophene):fullerene blends during the printing

---

process was achieved, which yielded a power conversion efficiency of 3–3.5% [31,32]. Other recent papers have also reported PCEs for inkjet printed RR-P3HT:PCBM OPVs exceeding 3% by using additives and combinations of different solvents [33,34].

Despite the recent progress in the field of inkjet printed OPVs, the influence of processing parameters on device PCE has not been investigated in the literature. The only previously published data focusing on processing conditions investigate drop spacing and pulse voltages and report a very low PCE in the range of $8 \times 10^{-4}$% [35].

In this paper we present details on the processing conditions solution viscosity, substrate temperature, drop spacing and nozzle-to-substrate distance. We show that the choice of parameters are critical to achieving high power conversion efficiency inkjet printed OPVs. Analysis in terms of one-diode equivalent circuit combined with current–voltage characteristics of the devices was performed to reveal the dominant loss mechanisms of the inkjet printed solar cells using these different processing conditions, whereby the device performance analyses help us to identify suitable processing conditions for inkjet printed organic solar cells. By using commercially available materials and a piezoelectric inkjet printer, the optimized printing process can produce OPVs with power conversion efficiency of 3.07%. This is a PCE similar to that achieved with conventional spin coating and doctor blading processing methods.

## 2. Experimental

The application of printing technology as a fabrication tool for organic photovoltaics indicates the potential of these novel materials for future light-activated plastic power sources. One of the key advantages of the inkjet printing technique is the use of Drop-On-Demand (DOD) technology. The controlled deposition of the solution on specific locations on the substrate eliminates the need of patterning for the production of OPV modules. For the trials reported in this paper ortho-dichlorobenzene (o-DCB) was used as a solvent. The deposition of the RR-P3HT:PCBM layer was performed by using a commercial piezoelectric driven inkjet head with a motorized xyz stage, a fiducial camera for substrate alignment and a drop watcher camera to control the drop shape.

RR-P3HT with average molecular weight of 50 kg mol$^{-1}$ and ~95% regioregularity was purchased from Rieke materials, [6,6]-phenyl C61 butyric acid methyl ester (PCBM) from nano-C and the evaporated metal Ca/Ag top electrode materials purchased from Aldrich. Thickness measurements of the deposited layers were performed with a Veeco Dektak 150. A Keithley 2420 source meter was used for the current density vs. voltage characteristics ($J/V$). The active layer was deposited with a Dimatix Fujifilm DMP 2831 inkjet printer using 254 μm nozzle spacing and 1 pL droplet volume cartridges.

15 mg RR-P3HT and 12 mg PCBM were diluted separately in pristine o-DCB (solvent amount varied as indicated in Fig. 1a) and stirred overnight at 85 °C. After approximately 12 h the two separated solutions were mixed and stirred at 85 °C until solution homogeneity was achieved. Before inserting the mixture into the cartridge, the ink-formulation was filtered with a 0.2 μm teflon filter and left in a vertical position for 30 min to remove air bubbles which could interfere in the printing process. The cartridge temperature was set at 66 °C to achieve the appropriate solution viscosity essential to avoid nozzle clogging. The droplet firing voltage was set at 11 V, the tickle control frequency at 5 Hz, meniscus at 5 in. H$_2$O, slew rate at 0.6 and duration at 3.8 μs. The above parameters provide uniform droplets with large ligaments for the ink-formulations.

RR-P3HT:PCBM blends were printed on top of a 50 nm doctor bladed PEDOT:PSS (Baytron AL4083) buffer layer. Glass/ITO transparent substrate/electrodes were used for all the devices reported. The total printed area on each substrate was 1 cm$^2$ and through a shadow mask 10 nm of calcium and 100 nm of silver were thermally evaporated in order to form the cathode for four OPV devices of $(9 \pm 0.05)$ mm$^2$ active layer each. For the needs of this study, more than 100 devices were fabricated and analyzed. In order to avoid any oxidation/degradation of the active layer, thermal annealing treatment of 15 min at 140 °C was performed inside a nitrogen-filled glove box. $J/V$ characteristics under illumination were also measured in these conditions but due to lack of a solar simulator providing 100 mW/cm$^2$ inside the glovebox a smaller white light source of 12 mW/cm$^2$ was preferred.

## 3. Results and discussion

To investigate the effect of viscosity on the inkjet printed OPVs, RR-P3HT:PCBM in a 1:0.8 (w:w) ratio was diluted in 1 and 0.5 mL of pristine o-DCB, providing solutions with two different printable viscosities. While exact viscosity values have not been calculated for this series, the values lie within the jettable range for printing provided by the manufacturer (2–30 mPa s) as no nozzle clogging issues were encountered. Fig. 1 (upper plot) shows the effect of viscosity on the $J/V$ characteristics under illumination, while Table 1 summarizes the device performance parameters collected for these
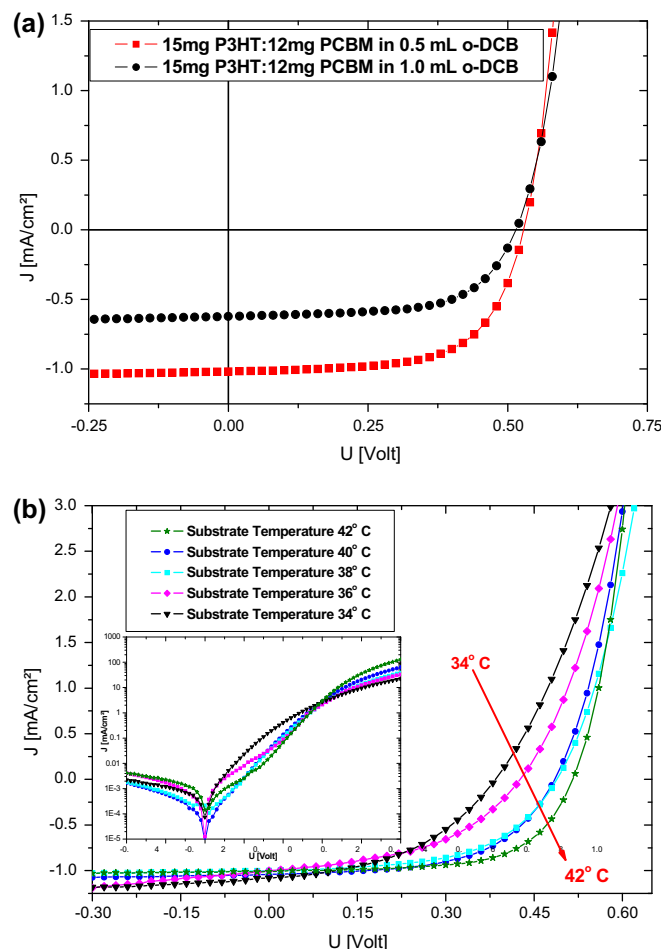


**Fig. 1.** Upper plot (a) $J/V$ characteristics under illumination represent the effect of solution viscosity on the inkjet printed OPV device performance. Bottom plot (b) $J/V$ characteristics under illumination represent the effect of substrate temperature on the device performance of RR-P3HT:PCBM based OPVs.

**Table 1**
Overview of the inkjet printed organic solar cells PCE device parameters obtained by different inkjet printing processing parameters (solution viscosity, surface temperature, drop spacing and nozzle-to-substrate distance).

| Inkjet printing processing parameters | $V_{oc}$ (V) | $J_{sc}$ (mA/cm$^2$) | FF | PCE (%) |
|---|---|---|---|---|
| RR-P3HT:PCBM 1:0.8 w:w in 1.0 mL o-DCB | 0517 | 0569 | 0631 | 1.55 |
| RR-P3HT:PCBM 1:0.8 w:w in 0.5 mL o-DCB | 0528 | 1017 | 0637 | 2.63 |
| *RR-P3HT:PCBM 1:0.8 w:w in 0.5 mL o-DCB* | | | | |
| Substrate temperature 34 °C | 0384 | 1081 | 0447 | 1.52 |
| Substrate temperature 36 °C | 0426 | 1002 | 0465 | 1.63 |
| Substrate temperature 38 °C | 0493 | 0935 | 0569 | 2.13 |
| Substrate temperature 40 °C | 0484 | 1042 | 0562 | 2.34 |
| Substrate temperature 42 °C | 0515 | 1011 | 0627 | 2.68 |
| *RR-P3HT:PCBM 1:0.8 w:w in 0.5 mL o-DCB* | | | | |
| *Substrate temperature 42 °C* | | | | |
| Drop spacing 15 µm | 0469 | 0911 | 0359 | 1.16 |
| Drop spacing 10 µm | 0529 | 1101 | 0625 | 2.76 |
| Drop spacing 5 µm | 0530 | 1212 | 0632 | 3.07 |
| *RR-P3HT:PCBM 1:0.8 w:w in 0.5 mL o-DCB* | | | | |
| *Substrate temperature 42 °C* | | | | |
| *Drop spacing 5 µm* | | | | |
| Nozzle-to-sample distance 1400 µm | 0542 | 1187 | 0563 | 2.74 |
| Nozzle-to-sample distance 1200 µm | 0531 | 1212 | 0632 | 3.07 |

two ink formulations. As can be seen from Table 1, the higher PCE is obtained from the more viscous solution, which provides thicker active layers with higher photocurrent values. Despite this increase in thickness the fill factor (FF) value of 0.63 was not affected, suggesting that the thicker layer still has adequate transport properties and no dominant recombination losses for efficient charge collection are present.

Similarly, the open circuit voltage ($V_{oc}$) was also not affected (0.52 V) by using a more viscous solution, indicating that the thickness of the active layer was close to the predicted optimum value [36]. The higher viscosity solution (RR-P3HT:PCBM 1:0.8 w:w diluted in 0.5 mL pristine o-DCB) resulted in inkjet printed OPVs with a PCE in the range of 2.6%. This is due to a higher amount of photons being absorbed by the active layer, as approximately double the thickness (in the range of 250 nm) was achieved as opposed to the less viscous solution.

We note that investigations of the photovoltaic performance for higher solution viscosities was also performed but in keeping with previously reported observations the small amount of solvent in each droplet mainly affected the printing ability, due to nozzle clogging [37,38].

Having established the better performing RR-P3HT:PCBM mixture's viscosity, the substrate temperature and its effect on the drying rate of the solvent formulation was investigated. Fig. 1 (bottom plot) shows this effect of substrate temperature on the $J/V$ characteristics under illumination. Under no temperature addition of the substrate the high boiling point of o-DCB of around 180 °C will cause a slow solvent evaporation rate, resulting in non-uniform film formation and high surface roughness active layers [28]. The evaporation rate is affected by the substrate temperature and the experimental results presented below indicate that the chosen substrate temperature is important for high PCE inkjet printed OPVs. After printing the desired pattern on every substrate, the inkjet printer's lid was left open so that the vapor pressure of the solvent would not affect the drying process. Previous trials using pristine high boiling solvents such as tetralene showed losses in the short circuit current ($J_{sc}$) and $V_{oc}$, which were identified as losses due to morphological issues and recombination mechanisms within the deposited active layer [28].

Table 1 summarizes the OPV device parameters obtained as a function of substrate surface temperature. $V_{oc}$ and FF linearly improve from 0.38 to 0.52 V and 0.45 to 0.63, respectively, as the substrate temperature rises from 34 to 42 °C. This suggests that

modification of the solvent evaporation rate by temperature can be used to control drying speed and increase polymer crystallization, resulting in larger domains of the blend materials and thus improving the morphology during the inkjet printing process. The best PCE of 2.7% was achieved at 42 °C substrate temperature. Above 42 °C we observed undesirable topography for the active layer, because at this temperature the solvent evaporates mainly from the droplet's boundaries. Thus, the direction of liquid flow is from the center towards the edges, resulting in ring-like active layers.

Having now established suitable substrate temperature and solution viscosity, the next inkjet printing processing parameter under investigation was drop spacing. Fig. 2 shows representative $J/V$ characteristics in the dark (upper plot) and under illumination (bottom plot) as a function of drop spacing conditions. The dark $J/V$ characteristics as a function of drop spacing reveal that despite the fact that in negative polarity and low positive bias the three devices fabricated with different drop spacing conditions behave similarly, differences are observed above 0.45 V.

In a macroscopic device model and at the high voltage linear regime of the dark $J/V$ characteristics, the current flowing through the device is limited by the series resistance ($R_s$) [39]. The slope of the dark $J/V$ at 1 V for the devices that were fabricated with 15 µm drop spacing indicates transport limitations, mainly limiting the FF value (see Fig. 2 bottom plot) and to a lesser extent the $J_{sc}$ values [40,41]. The poor $J/V$ characteristics under illumination (Fig. 2 bottom plot) of 15 µm drop spacing (DS15) devices is due to the inhomogeneity of the RR-P3HT:PCBM inkjet-printed active layer since drop merging is only partial.

As the inkjet printer deposits with cartridge angle 3.4° and DS15, the diluted mixture was printed in horizontal lines and solidified before it could form a homogenous layer. Therefore, a uniform RR-P3HT:PCBM active layer cannot be achieved for DS15. On the other hand, printing trials with drop spacing of 5 µm (DS5) and 1.1° as well as drop spacing of 10 µm (DS10) with 2.3° achieved merged inkjet printed active layers. The slightly improved performance with DS5 drop spacing is due to an improved photocurrent value as well as good layer thickness of around 350 nm – a thickness value close to the optimum for inkjet printed RR-P3HT:PCBM blends diluted in pristine o-DCB.

To summarize the inserted scheme of Fig. 2 (bottom plot), for DS15 the drop distance of 15 µm exceeds the solution's wettability and the drops never have contact in order to form a homogenous
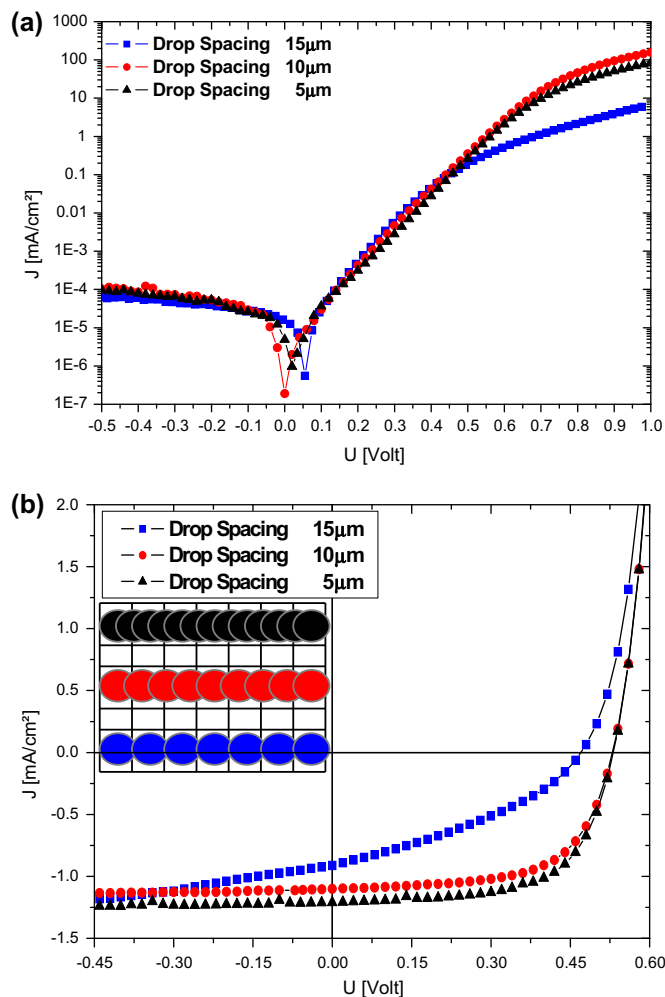
**Fig. 2.** Upper plot (a) dark current density vs. voltage characteristics in log/linear representation for different drop spacing values (5–15 μm). Bottom plot (b) *J*/*V* characteristics under illumination when drop spacing varied from 5 to 15 μm. The inset of Fig. 2 (bottom plot) provides a schematic explanation of the variation of drop spacing and its effect on the resulting active layer film quality.

layer. For DS5 and DS10 drop spacing values, the drops mix adequately. Since with DS5 more drops partly or totally cover one pixel and the solution volume per unit area is higher, a significantly thicker active layer is obtained. The achieved thickness for DS5 drop spacing was close to 350 nm resulting in predicted IQE values in the range of 95% [23,42].

The above results show that the selection of the appropriate drop spacing and cartridge angle at a certain ink viscosity and temperature (to control the evaporation rate of the solvent), can be used to adjust the layer thickness of inkjet printed polymer:fullerene OPVs. The device parameters in Table 1 show a PCE of 3.07% for 5 μm drop spacing devices. FF values reported for 5 and 10 μm drop spacing are also good (63%), dramatically reducing to 36% for 15 μm drop spacing. The observed short circuit current differences for the three devices under investigation are due to differences in the active layer thickness as explained in more detail above.

Though no current flows through the series resistance at open circuit conditions and no $V_{oc}$ reduction is observed as expected for 5 and 10 μm drop spacing devices, the devices fabricated with DS15 showed a reduced $V_{oc}$ value of 470 mV, due to a non-uniform active layer. BHJ inkjet printed OPVs with high PCE using pristine solvent formulations have been reported in the literature [34,43].

The highest PCE of 3.07% presented in this work was achieved with 5 μm drop spacing (DS5).

The final inkjet-printed processing condition under investigation was the nozzle-to-substrate distance. Fig. 3 shows representative *J*/*V* measurements in the dark (upper plot) and under illumination (inserted plot) for nozzle-to-substrate distances of 1200 μm (circles) and 1400 μm (squares) and with the optimum value of 5 μm drop spacing, substrate temperature of 42 °C and chosen solution viscosity (RR-P3HT:PCBM 1:0.8 w:w diluted in 0.5 mL of pristine o-DCB).

The dark *J*/*V* characteristics show that the selection of nozzle-to-substrate distance clearly affects the slope of the dark *J*/*V* at 1 V, indicating an influence on the active layer transport properties [39]. The major impact of transport limitations is noticeable in the reduced FF of the 1400 μm nozzle-to-substrate distance devices. As the droplets are deposited on the substrate they create a layer with solidified grains stacked one on top of the other. Fast drying of these droplets results in a multi "bi-layer" type structure, which provides slightly higher $V_{oc}$ value but at the same time less efficient transport properties; reflected in the reduced FF obtained. Thus, the illuminated *J*/*V* characteristics in Fig. 3 (inserted plot), show limited PCE performance for the devices with 1400 μm nozzle-to-substrate distance.

When the solution droplet is released from higher than the optimized distance, it solidifies at a certain degree providing
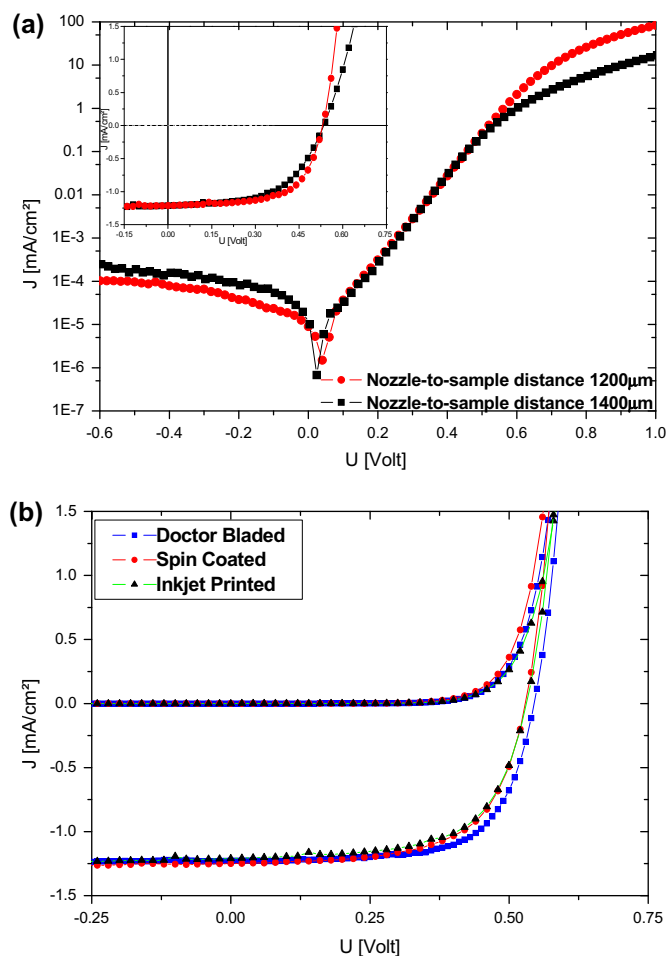


**Fig. 3.** Upper plot (a) *J*/*V* characteristics in dark (main) and under illumination (inset) when the nozzle-to-substrate distance was altered from 1200 to 1400 μm. Bottom plot (b) *J*/*V* characteristics in dark and under illumination for OPVs processed by inkjet printed in comparison to reference optimized spin coated and doctor bladed OPVs.

**Table 2**
Overview of PCE device parameters for optimized organic solar cells processed by inkjet printing, in comparison to optimized spin coated and doctor bladed OPVs. For all the devices presented the $J/V$ characteristics under illumination were measured at low light intensity.

| Processing method | $V_{oc}$ (V) | $J_{sc}$ (mA/cm$^2$) | FF | PCE (%) |
|---|---|---|---|---|
| Inkjet printing | 0530 | 1212 | 0632 | 3.07 |
| Spin coating | 0528 | 1322 | 0627 | 3.31 |
| Doctor blading | 0545 | 1299 | 0670 | 3.58 |

non-favorable morphology for the active layers. The low FF value obtained for the 1400 μm distance of droplet from substrate indicates morphological limitations and low charge carrier collection properties under this condition. The device performance data summarized in Table 1 show that a nozzle-to-substrate distance of 1200 μm is essential for reaching high OPV performance.

To confirm that the above processing conditions described for inkjet printed OPVs are close to optimum values, the $J/V$ characteristics were compared to RR-P3HT:PCBM OPVs prepared with optimized conditions in our labs with spin coating and doctor blading techniques using chloroform/chlorobenzene solvent mixture [44] and pristine chlorobenzene, respectively. Fig. 3 shows representative $J/V$ in the dark and under illumination (bottom plot) and Table 2 summarizes device performance for OPVs fabricated using the above three processing methods. The device performance for all the processing methods is within 3.1–3.6%. The doctor blading cells mainly have higher FF and the spin coated OPVs have higher $J_{sc}$ compared to the inkjet printed solar cells. We attribute these differences to the small adjustments to thickness and morphological properties of the inkjet printed active layer, necessary because of the more restricted processing conditions applied during the inkjet printing process.

## 4. Conclusions

The technological attraction in organic electronic applications is their suitability for printing processes. In this contribution, we have described in detail the processing conditions of inkjet printed active layers comprising a blend of RR-P3HT:PC$_{61}$BM using o-DCB solvent. We have shown that solution viscosity, substrate temperature, drop spacing and droplet height are critical parameters for optimized inkjet-printed active layer processing. Considering these parameters, it is shown that efficient inkjet-printed OPVs can be achieved with commercially available materials and pristine solvent formulation. We believe that the above results can be used to provide initial reference processing conditions for inkjet-printed organic electronic applications using polymer–fullerene blend active layers.

## References

[1] C.J. Brabec, N.S. Sariciftci, J.C. Hummelen, Adv. Funct. Mater. 11 (2001) 15–26.

[2] H. Spanggaard, F.C. Krebs, Sol. Energy Mater. Sol. Cells 83 (2004) 125–146.
[3] K.M. Coakley, M.D. McGehee, Chem. Mater. 16 (2004) 533–4542.
[4] H. Hoppe, N.S. Sariciftci, J. Mater. Res. 19 (2004) 1924–1945.
[5] C.J. Brabec, J.A. Hauch, P. Schilinsky, C. Waldauf, MRS Bull. 30 (2005) 50–52.
[6] F.C. Krebs, Refocus 6 (2005) 38–39.
[7] R. Kroon, M. Lenes, J.C. Hummelen, P.W.M. Blom, B. de Boer, Polym. Rev. 48 (2008) 531–582.
[8] G. Li, V. Shrotriya, J. Huang, Y. Yao, T. Moriarty, K. Emery, Y. Yang, Nat. Mater. 4 (2005) 864–868.
[9] W. Ma, C. Yang, X. Gong, K. Lee, A.J. Heeger, Adv. Funct. Mater. 15 (2005) 1617–1622.
[10] Y. Liang, Z. Xu, J. Xia, S.-T. Tsai, Y. Wu, G. Li, C. Ray, L. Yu, Adv. Mater. 22 (2010) E135–E138.
[11] H.-Y. Chen, J. Hou, S. Zhang, Y. Liang, G. Yang, Y. Yang, L. Yu, Y. Wu, G. Li, Nat. Photonics 3 (2009) 649–653.
[12] S.H. Park, A. Roy, S. Beaupre', S. Cho, N. Coates, J.S. Moon, D. Moses, M. Leclerc, K. Lee, A.J. Heeger, Nat. Photonics 3 (2009) 297–302.
[13] V.D. Mihailetchi, H. Xie, B. de Boer, L.M. Popescu, J.C. Hummelen, P.W.M. Blom, L.J.A. Koster, Appl. Phys. Lett. 89 (2006).
[14] W. Ma, J.Y. Kim, K. Lee, A.J. Heeger, Macromol. Rapid Commun. 28 (2007) 1776–1780.
[15] X. Yang, J. Loos, S.C. Veenstra, W.J.H. Verhees, M.M. Wienk, J.M. Kroon, M.A.J. Michels, R.A.J. Janssen, Nano Lett. 5 (2005) 579–583.
[16] A.J. Mouli, K. Meerholz, Adv. Mater. 20 (2008) 240–245.
[17] Y. Kim, S. Cook, S.M. Tuladhar, S.A. Choulis, J. Nelson, J.R. Durrant, D.C. Bradley, M. Giles, I. McCulloch, C.-S. Ha, M. Ree, Nat. Mater. 5 (2006) 197–203.
[18] J.A. Renz, T. Keller, M. Schneider, S. Shokhovets, K. Jandt, G. Gobsch, H. Hoppe, Sol. Energy Mater. Sol. Cells 93 (2009) 508–513.
[19] W. Ma, C. Yang, X. Gong, K. Lee, A.J. Heeger, Adv. Funct. Mater. 15 (2005) 1617–1622.
[20] G. Li, Y. Yao, H. Yang, V. Shrotriya, G. Yang, Y. Yang, Adv. Funct. Mater. 17 (2007) 1636–1644.
[21] S.S. van Bavel, M. Barenklau, G. de With, H. Hoppe, J. Loos, Adv. Funct. Mater. 20 (2010) 1458–1463.
[22] M. Campoy-Quiles, T. Ferenczi, T. Agostinelli, P.G. Etchegoin, Y. Kim, T.D. Anthopoulos, P.N. Stavrinou, D.D.C. Bradley, J. Nelson, Nat. Mater. 7 (2008) 158–164.
[23] G. Dennler, M.C. Scharber, C.J. Brabec, Adv. Mater. 21 (2009) 1323–1338.
[24] S.H. Jin, B.V.K. Naidu, H.-S. Jeon, S.-M. Park, J.-S. Park, S.C. Kim, J.W. Lee, Y.-S. Gal, Sol. Energy Mater. Sol. Cells 91 (2007) 1187–1193.
[25] C. Girotto, D. Moia, B.P. Rand, P. Heremans, Adv. Funct. Mater. 21 (2011) 64–72.
[26] C. Girotto, B.P. Rand, J. Genoe, P. Heremans, Sol. Energy Mater. Sol. Cells 93 (2009) 454–458.
[27] S.I. Na, B.K. Yu, S.S. Kim, D. Vak, T.S. Kim, J.S. Yeo, D.Y. Kim, Sol. Energy Mater. Sol. Cells 94 (2010) 1333–1337.
[28] C.N. Hoth, P. Schilinsky, S.A. Choulis, C.J. Brabec, Macromol. Symp. (2010) 287–292.
[29] F.C. Krebs, Sol. Energy Mater. Sol. Cells 93 (2009) 394–412.
[30] M. Singh, H.M. Haverinen, P. Dhagat, G.E. Jabbour, Adv. Mater. 22 (2010) 673–685.
[31] C.N. Hoth, P. Schilinsky, S.A. Choulis, C.J. Brabec, Nano Lett. 8 (2008) 2806–2813.
[32] C.N. Hoth, P. Schilinsky, S.A. Choulis, C.J. Brabec, Adv. Mater. 19 (2007) 3973–3978.
[33] S.H. Eom, H. Park, S.H. Mujawar, S.C. Yoon, S.S. Kim, S.I. Na, S.J. Kang, D. Khim, D.Y. Kim, S.H. Lee, Org. Electronics 11 (2010) 1516–1522.
[34] A. Lange, M. Wegener, C. Boeffel, B. Fischer, A. Wedel, D. Neher, Sol. Energy Mater. Sol. Cells 94 (2010) 1816–1821.
[35] V. Fauzia, A.A. Umar, M.M. Salleh, M. Yahya, Optimization of inkjet printing technique parameters for fabrication of bulk heterojunction organic solar cells, in: IEEE International Conference on Semiconductor Electronics, Proceedings, ICSE, 2010, pp. 60–63.
[36] K.M. Coakley, M.D. Mcgehee, Chem Mater. 16 (2004) 4533–4542.
[37] J. Perelaer, P.J. Smith, E. van den Bosch, S.S.C. van Grootel, P.H.J.M. Ketelaars, U.S. Schubert, Macromol. Chem. Phys. 210 (2009) 495–502.
[38] J. Perelaer, P.J. Smith, M.M.P. Wijnen, E. van den Bosch, R. Eckardt, P.H.J.M. Ketelaars, U.S. Schubert, Macromol. Chem. Phys. 210 (2009) 387–393.
[39] C. Waldauf, M.C. Scharber, P. Schilinsky, J.A. Hauch, C.J. Brabec, Appl. Phys. 99 (2006).
[40] J.D. Servaites, S. Yeganeh, T.J. Marks, M.A. Ratner, Adv. Funct. Mater. 20 (2010) 97–104.
[41] J. Nelson, The Physics of Solar Cells, Imperial College Press, London, England, 2003.
[42] G. Dennler, K. Forberich, M.C. Scharber, C.J. Brabec, J. Appl. Phys. 102 (2007).
[43] S.H. Eom, S. Senthilarasu, P. Uthirakumar, S.C. Yoon, J. Lim, C. Lee, H.S. Lim, J. Lee, S.H. Lee, Org. Electron. 10 (2009) 536–542.
[44] Y.S. Kim, Y. Lee, J. Kim, E.O. Seo, E.W. Lee, W. Lee, S.-H. Han, S.-H. Lee, Curr. Appl. Phys. 10 (2010) 985–989.